applied sciences

MDPI

Article

Properties of Spatially Indirect Excitons in Nanowire Arrays

Vladimir N. Pyrkov [1] and Victor M. Burlakov [2,*]

[1] Space Research Institute, Russian Academy of Sciences (IKI), 84/32 Profsoyuznaya Str., 117997 Moscow, Russia; pyrkov@mail.ru
[2] Linacre College, University of Oxford, St. Cross Road, Oxford OX1 3JA, UK
* Correspondence: victor.burlakov@linacre.ox.ac.uk

Featured Application: Determining parameters of spatially indirect excitons in semiconductor nanowires for nanoelectronics.

Abstract: This paper deals with the excitons formed by electrons and holes located in different, closely placed semiconducting nanowires (spatially indirect excitons). We calculated the charge densities and the binding energies of the excitons for different nanowire diameters D and distances h between the nanowires. Together with the estimated exciton lifetimes, these results suggest that at certain h and D, the spatially indirect excitons in the nanowire arrays may have the potential to serve as information-processing units. Possible ways of exciton generation in the nanowire arrays are discussed.

Keywords: spatially indirect excitons; nanowires; binding energy; electron tunneling; exciton dissociation

Citation: Pyrkov, V.N.; Burlakov, V.M. Properties of Spatially Indirect Excitons in Nanowire Arrays. *Appl. Sci.* **2022**, *12*, 4924. https://doi.org/10.3390/app12104924

Academic Editor: Francesco Tornabene

Received: 16 April 2022
Accepted: 10 May 2022
Published: 12 May 2022

Publisher's Note: MDPI stays neutral with regard to jurisdictional claims in published maps and institutional affiliations.

Copyright: © 2022 by the authors. Licensee MDPI, Basel, Switzerland. This article is an open access article distributed under the terms and conditions of the Creative Commons Attribution (CC BY) license (https://creativecommons.org/licenses/by/4.0/).

1. Introduction

Unprecedented progress in the fabrication of semiconductor nanowires (NWs) has stimulated their application in various areas, such as nano- and optoelectronics [1–4], photovoltaics (PV) [5,6], random lasers [7,8], etc. NWs have been used as building blocks for fabricating various nanodevices including FETs [1,9], p-n diodes, and inverters [1,2]. These NW devices can be assembled in a predictable way and methods exist for their parallel assembly [1,10]. The control of NW sizes achieved by a number of growth mechanisms including the widely used vapour–liquid–solid (VLS) process [11,12] also allows for the study of exciton properties confined in two dimensions, with various degree of confinement. The Coulomb interaction between an electron and a hole located in neighbouring NWs may at certain conditions result in the bound state called 'spatially indirect exciton' (SIE) [13–15]. The controlled arrangement of NWs into three dimensional ordered structures might potentially allow generating arrays of SIEs, the properties of which would be very interesting to investigate.

Spatially indirect excitons are thought to be more long-lived than the usual (direct) excitons because of the spatial separation of electrons and holes [16–18]. They have been discussed in conjunction with quantum Bose gas in quasi-2D systems [13,19,20], capacitance in layered transition metal dichalcogenide structures [18,21], and as the information units in quantum posts [22,23]. So far, SIEs have been considered either for flat interfaces (the 2D case), or in pairs of quantum dots, the so-called quantum posts (the 0D case). In this article, we consider SIEs formed in parallel NWs (the 1D case) and analyse their binding energy and lifetime as functions of the NW diameter.

2. Results and Discussion

2.1. Binding Energy and Charge Distribution for SIEs

Consider an electron and hole located in parallel NWs of a diameter D separated by the distance h between their surfaces. The Coulomb interaction between the charges

mediates the formation of spatially indirect excitons. The binding energy E_x of such SIEs as a function of D obtained by direct quantum mechanical calculations (see Appendix A) for different values of h is shown in Figure 1. The value of E_x at h = 1 nm and D = 1.5 nm slightly exceeds 100 mV, which is close to the binding energy of the Hybrid Charge Transfer Excitons at the organic–inorganic interface [24]. An increase in h understandably results in a noticeable decrease of E_x for all NW diameter values D. It is worth pointing out the strong dependence of E_x upon D in the range of $D < 10$ nm and its levelling up at high D-values for all values of h. The steep decrease in E_x at low D-values can be understood in terms of the charge density delocalization for the electron and hole across the corresponding NWs. Indeed, the strong confinement in the narrower NWs makes the charges look more point-like, and results in a stronger interaction between them and hence in a higher E_x. The non-monotonic behaviour of $E_x(D, h = 3)$ at low D-values is most likely due to some minor transformation in the charge distributions. Delocalization of the charges in relatively thick NWs makes them look more like clouds and results in levelling up $E_x(D \to \infty, h)$ down to the values characteristic for flat interfaces and determined by the spacing h. It was found that the binding energies for SIEs in the crossed NWs are very close to those presented above.

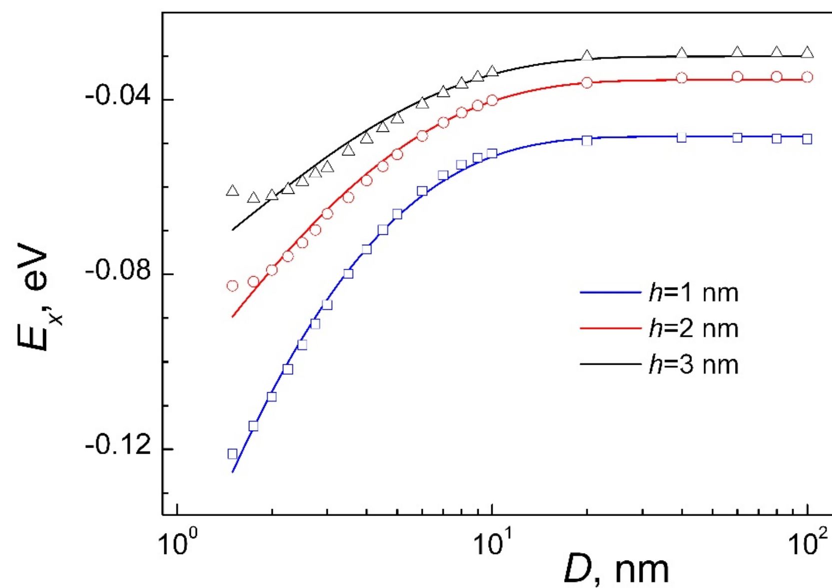

Figure 1. Binding energy E_x of the SIE formed by an electron and hole located in neighbouring parallel NWs of diameter D separated by the distance h. Symbols (triangles, circles, and squares) –results of calculations for $m_h = 5 \cdot m_e$ and effective dielectric constant $\varepsilon = 4$, as described in Appendix A. Solid lines show the corresponding approximations by Equation (1) (see text) with the fit parameters: α = 6.4 nm, β = 0.23 nm^{-1} for h = 1 nm; α = 8.1 nm, β = 0.19 nm^{-1} for h = 2 nm; and α = 8.9 nm, β = 0.18 nm^{-1} for h = 3 nm.

The outlined qualitative picture is illustrated by the charge density distributions shown in Figure 2. According to the figure, the charge densities in narrow NWs (panels A and B) are localized, while they are much more extended in the thicker NWs (panels C and D). This change in charge density localization for h = 1 (compare the panels A and C) significantly affects the binding energy-see the blue symbols in Figure 1-while for h = 3 (panels B and D), it creates a much smaller effect—see the black symbols in Figure 1. Based on the obtained results, it is useful to approximate the SIE binding energy $E_x(D, h)$ with the following ad hoc analytical expression

$$E_x(D, h) = \frac{A}{h + \alpha \cdot (1 - \exp(-\beta \cdot D))}, \; A = \frac{e^2}{4\pi\varepsilon_0\varepsilon} = 0.359 \text{ eV} \cdot \text{nm} \quad (1)$$

where e stands for the electronic charge, $\varepsilon_0\varepsilon$ is an effective dielectric constant ($\varepsilon = 4$) of the NW-vacuum spacing-NW system, and α and β are the fit parameters. The fitting function in Equation (1) is constructed considering the fact that the system of two parallel NWs with constant inter-NW distance and increasing diameters D is converted, according to parameter β, into a flat interface. Then, the binding energy between the electron and hole would be simply a Coulomb potential with some effective electron–hole distance, determined by the parameter α. According to Figure 1, the proposed analytical expression describes the calculation results quite well, suggesting that it can be used for estimating the SIE binding energies.

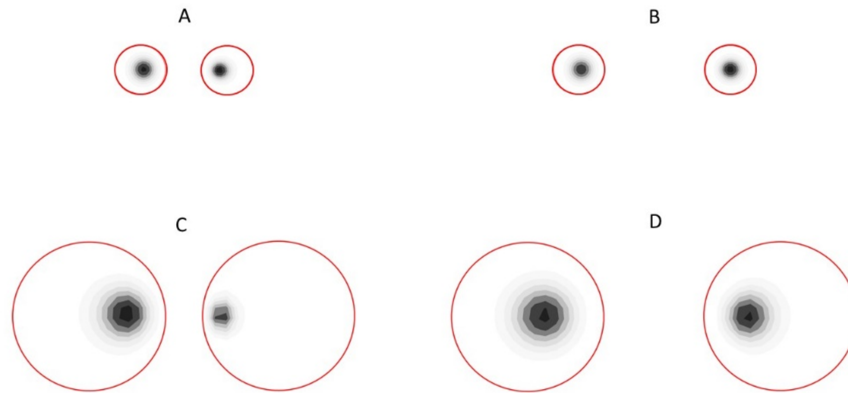

Figure 2. Charge densities of electron and hole across corresponding neighbouring parallel NWs of diameter D obtained by direct quantum mechanical calculations (see Appendix A) for different values of the NW diameter D and h. (**A**) h = 1 nm, D = 1.5 nm; (**B**) h = 3 nm, D = 1.5 nm; (**C**) h = 1 nm D = 5 nm; (**D**) h = 3 nm, D = 5 nm.

2.2. SIE Life Time

The lifetime of the SIE in the NWs is affected by (i) tunnelling of charges (predominantly electron) followed by electron–hole recombination, and (ii) exciton dissociation. The calculated (see Appendix A) tunnelling times are presented in Table 1 below.

Table 1. Tunnelling times τ_t for electrons from the home NW into the hole NW (see Appendix A) and exciton dissociation times τ_d estimated using Equation (2) for T = 77 K.

D, nm	h, nm	$\tau_t(D,h)$, s	$\tau_d(D,h)$, s
1.5	1.0	2×10^{-11}	5×10^{-6}
3.0	1.0	2×10^{-9}	5×10^{-8}
1.5	2.0	10^{-6}	4×10^{-8}
3.0	2.0	7×10^{-6}	4×10^{-9}

The dissociation times $\tau_d(D,h)$ can be estimated using the expression $\tau_d^{-1}(D,h) \approx \nu(D,h)\cdot\exp(-E_x(D,h)/k_BT)$, where $\nu(D,h)$ is the frequency of the exciton internal oscillations along the NWs, k_B is the Boltzman constant, and T is absolute temperature. Assuming for simplicity that these oscillations are harmonic, we can estimate the frequency as $\nu(D,h) = \sqrt{K/\mu}/2\pi$, where K is an effective harmonic force constant, and $\mu = m_e m_h/(m_e + m_h)$ is an effective exciton mass. The value of K can be estimated using Equation (1) with effective electron-hole spacing $h' = \sqrt{h^2 + x^2} \approx h + 0.5\cdot x^2/h$, where x is the electron-hole instantaneous distance along the NW (in equilibrium x = 0). Then, expanding the binding energy in a series of x-powers and retaining the first two terms, we obtain

$$E_x(D,h') \approx -\frac{A}{h+0.5\cdot x^2/h+\alpha\cdot(1-\exp(-\beta\cdot D))} \approx E_x(D,h) + \frac{1}{2}K\cdot x^2,$$
$$K = \frac{1}{h}\cdot\frac{(E_x(D,h))^2}{A}$$

With the help of this expression for K, we estimated the exciton dissociation time as a function of D and h for $m_h = 5m_e$ and $T = 77K$ $(\approx 0.0067 \text{ eV})$

$$\tau_d(D,h) = 1/\nu(D,h)\cdot \exp\left(\frac{E_x(D,h)}{k_B T}\right) \approx \frac{10^{-14}\sqrt{h[\text{nm}]}}{E_x(D,h)[\text{eV}]}\cdot \exp\left(\frac{E_x(D,h)}{k_B T}\right) \quad (2)$$

Corresponding values of $\tau_d(D,h)$ are presented in Table 1. If the tunnelling times determine the exciton recombination times, then, according to Table 1, the SIE's lifetime in the case of $D = 3$ nm and $h = 1$ nm is determined by recombination and is restricted to a few nanoseconds. Most likely, this value can be significantly increased by applying some bias voltage to the NWs [22,23]. In contrast, for h = 2, the exciton lifetime is determined by dissociation, which can be increased by decreasing the system's temperature. The spatially indirect excitons can be generated by a number of ways, e.g., by optical pumping [25,26], applying a strain gradient [27], and possibly, in analogy with superlattices [28], from ordinary excitons by applying a sufficiently high electric field to the NWs. Keeping in mind that the NW parameters can be predetermined during their fabrication and that the NWs can subsequently be arranged in various structures, there is a hope that SIEs can potentially be useful for information processing.

3. Conclusions

We calculated the binding energies of spatially indirect excitons in semiconductor NWs and estimated the exciton's lifetime. The binding energies are found to be in the range 0.02 ÷ 0.1 eV and strongly dependent on the NW diameter and inter-NW spacing for small (below 10 nm) diameter values. The SIE lifetimes are found to be in the range $10^{-11} \div 10^{-6}$ s, depending on the NW diameter and inter-NW spacing. Considering recent progress in controlling the NW parameters during the fabrication and assembling of NW structures, the obtained SIE parameters illustrate their significant potential for applications in nanoelectronics and information processing.

Author Contributions: Conceptualization, V.M.B. and V.N.P.; methodology, V.N.P.; formal analysis, V.N.P. and V.M.B.; writing—original draft preparation, V.M.B.; writing—review and editing, V.M.B. All authors have read and agreed to the published version of the manuscript.

Funding: This research received no external funding.

Institutional Review Board Statement: Not applicable.

Informed Consent Statement: Not applicable.

Conflicts of Interest: The authors declare no conflict of interest.

Appendix A

Appendix A.1. CIE Binding Energy

A rigorous treatment of the Coulomb interaction between electron and hole located in neighbouring NWs is rather complicated due to the difference in the dielectric constant of the NW material and the surrounding space. For estimating the binding energy, one can assume that the Coulomb interaction can be described with some effective dielectric constant. A further simplification can be made using another and much weaker approximation of effective isotropic masses for electron and hole, m_e and m_h, respectively. We also took into account the electron (hole) work function $B_{e(h)}$ for the NW material, such that we can write the overall potential $U_{e(h)}$ for electron (hole), which obviously is independent of z, the coordinate along the NW, as

$$U_{e(h)} = B_{e(h)}\cdot\Theta\left(\sqrt{\left(x_{e(h)} - X_{e(h)}\right)^2 + {y_{e(h)}}^2} - R\right)$$

where x ($x \perp y \perp z$) connects the NW centres X_e and X_h ($X_h - X_e = 2R + h$), Θ is the Heaviside step function, and $R = D/2$–is the NW radius. Separating the motion of electron and hole mass centre along the NWs as $z_{eh} = z_e - z_h$, we obtain a 5-dimensional stationary Schrödinger equation for relative electron–hole motion described by the wave function $\psi \equiv \psi(x_e, y_e, x_h, y_h, z_{eh})$

$$E \cdot \psi = -\frac{1}{2m_e}\Delta_e \psi - \frac{1}{2m_h}\Delta_h \psi + U_e \cdot \psi + U_h \cdot \psi - \frac{1}{2\mu}\frac{\partial^2}{\partial z_{eh}^2}\psi - \frac{e^2}{\varepsilon \cdot r_{eh}}\psi \tag{A1}$$

where $\Delta_{e(h)} = \frac{\partial^2}{\partial x_{e(h)}} + \frac{\partial^2}{\partial y_{e(h)}}$, $r_{eh} = \sqrt{(x_e - x_h)^2 + (y_e - y_h)^2 + z_{eh}^2}$ is the electron-hole separation, and ε is the effective dielectric constant. To solve this equation, we implemented the virtual lattice method [29]. The results of solving Equation (A1) for $m_h = 5m_e$, $B_e = 1$ eV, $B_h = B_e + E_g = 2$ eV (E_g is the band gap of the NW material) and various h-values as a function of D are presented in Figure 1.

Appendix A.2. Electron Tunnelling between the NWs

The recombination lifetime of the SIE was assumed to be determined by the tunneling of the electron between the NWs, thus neglecting the much slower tunneling rate of the heavy and much more localized hole. For estimating the tunneling time τ_t, we used an idea about oscillating probability to find the electron in one of two potential wells [30]. For simplicity, consider an electron tunneling between the two 1D potential wells separated by a potential barrier. The oscillations of the probability amplitude for the electron to be located in the one or the another potential well would take place with the period $T = 2\pi/\Delta E$, where ΔE is the splitting between the symmetric and anti-symmetric electronic states. We associate this period T with the decay time $\tau_t = T/4$ of the initial electronic state.

In our case, the problem is more complicated: besides non-symmetric potential wells associated with the NWs, there is also an attraction Coulomb potential between the electron and hole. Therefore, we first calculated the hole probability density $\rho_h(r_h)(r_h = \{x_h, y_h\})$ using the eigenfunctions of Equation (A1). Then, by integrating the overall probability density over the hole variables x_h and y_h, we obtained the stationary Schrödinger equation for the electron

$$\begin{aligned} &-\tfrac{1}{2m_e}\Delta\psi_i + \left(U - \tfrac{e^2}{\varepsilon}\int \tfrac{\rho_h(r_h)}{r_{eh}} dr_h\right) \cdot \psi_i = E_i \cdot \psi_i, \\ &U = B_e \cdot \left(1 - \Theta\left(\sqrt{(x - X_e)^2 + y^2} - R\right) - \Theta\left(\sqrt{(x - X_h)^2 + y^2} - R\right)\right) \end{aligned} \tag{A2}$$

The eigen values E_i and eigen functions $\psi(x, y, z)$ were determined using the virtual lattice method [29]. The four lowest eigen energy states of Equation (A2) were found to be localized in the hole-hosting (below referred to as 'right') NW because of the strong electron–hole attraction. The fifth eigen state is mainly localized in the initial electron-hosting NW referred to below as 'left'. We want to estimate the tunnelling time from the left NW to the right one. To do this, consider the wave function $\psi_l(x, y, z, t = 0)$, which is non-zero only inside and around the left NW. We are interested in the transformation of this initial wave function into those localized in the right NW, namely

$$\begin{aligned} &\psi_l(x, y, z, t) = \sum_{k=1}^{5} C_k \cdot \varphi_k(x, y, z) \cdot \exp[-i \cdot E_k \cdot t], \\ &C_k = \iiint\limits_{x,y,z=-\infty \cdots +\infty} \psi_l(x, y, z, 0) \cdot \varphi_k(x, y, z) dx dy dz, \\ &C_5^2 \approx 1, \;\; C_k^2 << 1 \;\; \text{if} \;\; k \neq 5 \end{aligned}$$

where $\psi_l(x, y, z, t = 0)$ is actually close to φ_5.

Omitting the higher-degree terms, we can write for the probability for the electron to remain in the left NW $P_l(t)$

$$P_l(t) = 1 - 4 \sum_{k=1...4} C_k^2 \cdot Sin^2\left(\frac{(E_k - E_5)\cdot t}{2}\right)$$

The electron in the initial state ψ_l can tunnel to any of the four states φ_i $(i = 1, \ldots, 4)$, which we will refer to as the tunnelling channels. Each such tunnelling channel reaches its maximum amplitude in the time period $\Delta t_i = \pi/\Delta E_i$, where $\Delta E_i = |E_i - E_5|$. The tunnelling time for each tunnelling channel can then be estimated by analogy with the 1D case of symmetric quantum wells [30], which has an additional factor C_i^2. Depending on the considered parameters, some of the tunnelling channels can dominate. For all parameters considered in this work, the dominant channels are those to the states φ_3 and φ_4. The estimates of the resultant tunnelling time $\tau_t = \left(\tau_3^{-1} + \tau_4^{-1}\right)^{-1}$ are presented in Table 1.

$$\tau_{ti} = 4\frac{C_i^2}{C_5^2} \cdot \frac{\pi}{\Delta E_i} \approx 4C_i^2 \cdot \frac{\pi}{\Delta E_i}$$

References

1. Duan, X.; Huang, Y.; Cui, Y.; Wang, J.; Lieber, C.M. Indium phosphide nanowires as building blocks for nanoscale electronic and optoelectronic devices. *Nature* **2001**, *409*, 66–69. [CrossRef] [PubMed]
2. Cui, Y.; Lieber, C.M. Functional Nanoscale Electronic Devices Assembled Using Silicon Nanowire Building Blocks. *Science* **2001**, *291*, 851–853. [CrossRef] [PubMed]
3. Colinge, J.-P.; Lee, C.-W.; Afzalian, A.; Akhavan, N.D.; Yan, R.; Ferain, I.; Razavi, P.; O'Neill, B.; Blake, A.; White, M.; et al. Nanowire transistors without junctions. *Nat. Nanotechnol.* **2010**, *5*, 225–229. [CrossRef] [PubMed]
4. Mongillo, M.; Spathis, P.; Katsaros, G.; Gentile, P.; De Franceschi, S. Multifunctional Devices and Logic Gates with Undoped Silicon Nanowires. *Nano Lett.* **2012**, *12*, 3074–3079. [CrossRef]
5. Shalan, A.E.; Barhoum, A.; Elseman, A.M.; Rashad, M.M.; Lira-Cantú, M. Nanofibers as Promising Materials for New Generations of Solar Cells. In *Handbook of Nanofibers*; Barhoum, A., Bechelany, M., Makhlouf, A., Eds.; Springer International Publishing: Cham, Switzerland, 2018; pp. 1–33.
6. Kim, T.-Y.; Lee, T.K.; Kim, B.S.; Park, S.C.; Lee, S.; Im, S.S.; Bisquert, J.; Kang, Y.S. Triumphing over Charge Transfer Limitations of PEDOT Nanofiber Reduction Catalyst by 1,2-Ethanedithiol Doping for Quantum Dot Solar Cells. *ACS Appl. Mater. Interfaces* **2017**, *9*, 1877–1884. [CrossRef] [PubMed]
7. Quochi, F. Random lasers based on organic epitaxial nanofibers. *J. Opt.* **2010**, *12*, 024003. [CrossRef]
8. Quochi, F.; Saba, M.; Cordella, F.; Gocalinska, A.; Corpino, R.; Marceddu, M.; Anedda, A.; Andreev, A.; Sitter, H.; Sariciftci, N.S.; et al. Temperature Tuning of Nonlinear Exciton Processes in Self-Assembled Oligophenyl Nanofibers under Laser Action. *Adv. Mater.* **2008**, *20*, 3017–3021. [CrossRef]
9. Cui, Y.; Duan, X.; Hu, A.J.; Lieber, C.M. Doping and Electrical Transport in Silicon Nanowires. *J. Phys. Chem. B* **2000**, *104*, 5213–5216. [CrossRef]
10. Huang, Y.; Duan, X.; Cui, Y.; Lauhon, L.J.; Kim, K.-H.; Lieber, C.M. Logic Gates and Computation from Assembled Nanowire Building Blocks. *Science* **2001**, *294*, 1313–1317. [CrossRef]
11. Wagner, R.S.; Ellis, W.C. Vapour-liquid-solid mechanism of single crystal growth. *Appl. Phys. Lett.* **1964**, *4*, 89. [CrossRef]
12. Wagner, R.S. *Whisker Technology*; Levitt, A.P., Ed.; Wiley Interscience: New York, NY, USA, 1970; ISBN 0471531502/9780471531500.
13. Combescot, M.; Combescot, R.; Dubin, F. Bose–Einstein condensation and indirect excitons: A review. *Rep. Prog. Phys.* **2017**, *80*, 066501. [CrossRef] [PubMed]
14. Madureira, J.R.; de Godoy, M.P.F.; Brasil, M.J.S.P.; Iikawa, F. Spatially indirect excitons in type-II quantum dots. *Appl. Phys. Lett.* **2007**, *90*, 212105. [CrossRef]
15. Merkl, P.; Mooshammer, F.; Steinleitner, P.; Girnghuber, A.; Lin, K.-Q.; Nagler, P.; Holler, J.; Schüller, C.; Lupton, J.M.; Korn, T.; et al. Ultrafast transition between exciton phases in van der Waals heterostructures. *Nat. Mater.* **2019**, *18*, 691–696. [CrossRef] [PubMed]
16. Rivera, P.; Schaibley, J.R.; Jones, A.; Ross, J.S.; Wu, S.; Aivazian, G.; Klement, P.; Seyler, K.; Clark, G.; Ghimire, N.; et al. Observation of long-lived interlayer excitons in monolayer MoSe2–WSe2 heterostructures. *Nat. Commun.* **2015**, *6*, 6242. [CrossRef]
17. Ceballos, F.; Bellus, M.Z.; Chiu, H.-Y.; Zhao, H. Ultrafast Charge Separation and Indirect Exciton Formation in a MoS2–MoSe2 van der Waals Heterostructure. *ACS Nano* **2014**, *8*, 12717–12724. [CrossRef]
18. Calman, E.V.; Fogler, M.M.; Butov, L.V.; Hu, S.; Mishchenko, A.; Geim, A.K. Indirect excitons in van der Waals heterostructures at room temperature. *Nat. Commun.* **2018**, *9*, 1895. [CrossRef] [PubMed]
19. Su, J.-J.; MacDonald, A. How to make a bilayer exciton condensate flow. *Nat. Phys.* **2008**, *4*, 799–802. [CrossRef]

20. Fogler, M.M.; Butov, L.V.; Novoselov, K. High-temperature superfluidity with indirect excitons in van der Waals heterostructures. *Nat. Commun.* **2014**, *5*, 4555. [CrossRef]
21. Sammon, M.; Shklovskii, B.I. Attraction of indirect excitons in van der Waals heterostructures with three semiconducting layers. *Phys. Rev. B* **2019**, *99*, 165403. [CrossRef]
22. Krenner, H.J.; Pryor, C.E.; He, J.; Petroff, P.M. A Semiconductor Exciton Memory Cell Based on a Single Quantum Nanostructure. *Nano Lett.* **2008**, *8*, 1750–1755. [CrossRef]
23. Rolon, J.E.; Ulloa, S. Coherent control of indirect excitonic qubits in optically driven quantum dot molecules. *Phys. Rev. B* **2010**, *82*, 115307. [CrossRef]
24. Cheng, C.-H.; Leon, D.C.; Li, Z.; Litvak, E.; Deotare, P.B. Energy Transport of Hybrid Charge-Transfer Excitons. *ACS Nano* **2020**, *14*, 10462–10470. [CrossRef] [PubMed]
25. Yan, M.; Rothberg, L.J.; Papadimitrakopoulos, F.; Galvin, M.E.; Miller, T.M. Spatially indirect excitons as primary photoexcitations in conjugated polymers. *Phys. Rev. Lett.* **1994**, *72*, 1104–1107. [CrossRef] [PubMed]
26. Donegá, C.D.M. Formation of nanoscale spatially indirect excitons: Evolution of the type-II optical character of CdTe/CdSe heteronanocrystals. *Phys. Rev. B* **2010**, *81*, 165303. [CrossRef]
27. Liu, Z.; Fu, X.; Zhang, D.-B. Strain gradient induced spatially indirect excitons in single crystalline ZnO nanowires. *Nanoscale* **2020**, *12*, 19083–19087. [CrossRef]
28. Tartakovskii, A.I.; Timofeev, V.B.; Lysenko, V.G.; Birkedal, D.; Hvam, J. Direct and spatially indirect excitons in GaAs/AlGaAs superlattices in strong magnetic fields. *J. Exp. Theor. Phys.* **1997**, *85*, 601–608. [CrossRef]
29. Pyrkova, O.A.; Pyrkov, V.N.; Vasilets, P.M. Development of Virtual Lattice Dynamics Method for Solving the Eigenvalue Problem of Three-Dimensional Elliptic Equation with a Multicenter Potential. In *Smart Modelling for Engineering Systems. Smart Innovation, Systems and Technologies*; Favorskaya, M.N., Favorskaya, A.V., Petrov, I.B., Jain, L.C., Eds.; Springer: Singapore, 2021; Volume 215. [CrossRef]
30. Khairutdinov, R.F.; Zamaraev, K.I.; Zhdanov, V.P. Tunneling Phenomena in Physics and Chemistry. In *Comprehensive Chemical Kinetics*; Compton, R.G., Ed.; Elsevier: Amsterdam, The Netherlands, 1990; Chapter 2; Volume 30, pp. 7–68, ISSN 0069-8040/9780444873644. [CrossRef]